Manuscript Number:

Title: Impact Strengthening of 3Y-TZP Dental Ceramic Root Posts

Article Type: SI: FAC VI

Corresponding Author: Dr. Andraž Kocjan,

Corresponding Author's Institution: Jozef Stefan Institute

First Author: Andraž Kocjan

Order of Authors: Andraž Kocjan; Anže Abram; Aleš Dakskobler

Abstract: 3Y-TZP ceramics is commonly used in restorative dentistry for fixed partial dentures as well as for implants, abutments and root posts. The stress-induced transformation toughening mechanism that provides advantageous mechanical properties encourages grinding and sandblasting of 3Y-TZP for better clinical performance. Such invasive mechanical surface treatments facilitate additional strengthening of ceramic as a result of the compressive residual stresses, but their exact origin of formation is not completely understood. The present work evaluated the effect of continuous impacting between 3Y-TZP root posts during 500-hour-long shaking on the extent of (sub)surface microstructural changes affecting the fracture strength. With the increase of shaking time the surface roughness decreased, where the grains were flattened and partially spalled. The observed 6-micrometre-thick altered subsurface region containing compressive residual stresses had contributed to systematic increase in fracture strength within large-numbered sample populations, however, only for those containing surface-type critical flaws introduced during de-moulding of green bodies.

Suggested Reviewers: Tanja Lube
tanja.lube@unileoben.ac.at

Marc Anglada
marc.j.anglada@upc.edu

Summary of Novel Conclusions

- Substantial impact strengthening of the 3Y-TZP root posts was triggered by 500-hour-long shaking experiment. The (sub)surface microstructural changes contributed to systematic increase in ceramic strength due to compressive stress formation.

Impact Strengthening of 3Y-TZP Dental Ceramic Root Posts

Andraž Kocjan, Anže Abram, Aleš Dakskobler

Abstract

3Y-TZP ceramics is commonly used in restorative dentistry for fixed partial dentures as well as for implants, abutments and root posts. The stress-induced transformation toughening mechanism that provides advantageous mechanical properties encourages grinding and sandblasting of 3Y-TZP for better clinical performance. Such invasive mechanical surface treatments facilitate additional strengthening of ceramic as a result of the compressive residual stresses, but their exact origin of formation is not completely understood. The present work evaluated the effect of continuous impacting between 3Y-TZP root posts during 500-hour-long shaking on the extent of (sub)surface microstructural changes affecting the fracture strength. With the increase of shaking time the surface roughness decreased, where the grains were flattened and partially spalled. The observed 6-micrometre-thick altered subsurface region containing compressive residual stresses had contributed to systematic increase in fracture strength within large-numbered sample populations, however, only for those containing surface-type critical flaws introduced during de-moulding of green bodies.

Keywords: zirconia; dental ceramics; phase transformation; microstructure; fracture strength

1. Introduction

Yttria-stabilised tetragonal zirconia polycrystalline (3Y-TZP) ceramics has established itself as a material of choice in all-ceramic fixed partial dentures (FPD) owing to excellent mechanical properties combined with enhanced aesthetic appearance compared to metals.[1] Increased strength and toughness are attributed to its ability to undergo a stress-induced martensitic phase transformation (*t-m*) of the thermodynamically metastable tetragonal grains into the stable monoclinic form, thereby developing transformation toughening mechanism in its fine-grained polycrystalline microstructure. Under applied stress, the propagating growth of the crack is inhibited on the account of the martensitic transformation of metastable tetragonal grains to the monoclinic variants stable at room temperature, associated with the volume increase [2].

The 3Y-TZP`s tetragonal phase metastability also has a detrimental side known as low-temperature degradation (LTD) or ageing, where the *t-m* transformation is triggered spontaneously in the humid environment. The hydrothermal ageing is a nucleation-propagation, stress-corrosion-type of mechanism exhibiting linear kinetics [3][4][5][6][7]. The process is accompanied by surface roughening, grain pull-outs and extensive micro-cracking. It was even shown that it may operate at temperatures as low as 37 °C over several years and at high and low partial pressures of water [8]. 3Y-TZP`s propensity towards LTD highly depends on the grain size and the extent of phase partitioning [9][10][11]. However, doping the 3Y-TZP structure with additional aliovalent dopant [12] or even a small amount of a silicate glassy phase [13] can hinder the LTD process tremendously. The exact clinical relevance of the ageing process for dental applications has yet to be established.

For the use in dentistry, the 3Y-TZP surfaces are commonly treated by grinding and polishing after sintering for final adjustments of the occlusion as well as by airborne-alumina-particle abrasion (also known as sandblasting) for cleaning and to improve bonding since 3Y-TZP exhibits much higher chemical inertness as compared to the glass-ceramic FDP`s [14] [15]. Such intense mechanical adjustments of the 3Y-TZP surfaces can potentially introduce strength limiting surface flaws affecting the damage tolerance of ceramics. Although the surface is severely damaged and plastically deformed [16], the flexural strength actually increases substantially on the account of the transformation-induced surface strengthening [17]. Strengthening by surface damage in metastable tetragonal zirconia has been described for both grinding and airborne-particle abrasion [18]. In addition, the ageing process of 3Y-TZP was shown to be delayed or hindered if the surface had been mechanically treated as a result of the evolution of residual surface compressive stresses [19] present in the altered subsurface region consisting of recrystallized nano-size grains and textured, constrained grains [7][20].

The airborne-particle abrasion induced compressive stresses were shown to be potentially annihilated by either thermal annealing step [21] or by the sufficiently long hydrothermal ageing process [7]. In the case of the latter, the annihilation was complete when the transformed subsurface layer thickness consisting of monoclinic zirconia phase and microcracks was equally thick as the altered subsurface zone under compressive stresses. Interestingly, in neither case did annihilation result in a dramatic drop of strength values as a consequence of the damaged surface since measured flexural strengths were still above 1 GPa.

3Y-TZP FDP`s may also be subjected to an uncontrolled type of mechanical damage, namely, wear or impact, during industrial fabrication processes, transportation and handling during dental laboratory and clinical procedures. In the light of these events, the present work aimed at evaluating the effect of continuous impacting between 3Y-TZP dental root posts that had occurred during up to 500-hour-long shaking in a Turbula® mixer on the extent of (sub)surface microstructural changes affecting the fracture strength. The (sub)surface microstructural changes were carefully analysed using XRD, FIB-SEM and AFM. The forces at fracture of 30 posts per group before and after shaking experiment were measured using a 3-point bending test. Weibull and fractographic analyses were also conducted.

2. Methods
2.1. Experimental set-up

3Y-TZP dental root posts fabricated by the low-pressure injection moulding (LPIM) technique were produced and provided by Vall-Cer d.o.o. After LPIM the samples were de-binded and sintered at 1550 °C for 2 hours. The posts that contain a coronal part with the retention rings for an easier core build-up and improved retentive performance [22] are presented in Figure 1. The diameter of the lower straight part, the lower widest ring and the length are 1.4, 1.9 and 17.5 mm, respectively. For each shaking experiment, 30 3Y-TZP dental root posts were placed into a plastic capsule with the height and diameter of 140 and 25 mm, respectively. The capsule containing posts was then mounted to Turbula® mixer and were then shaken for 2, 8, 20, 50, 100, 200 and 500 hours at 2 Hz rate. The as-sintered samples will be denominated as AS, while the shaken samples tH depending on the length of shaking time (t) (for example; 2H for samples shaked for 2 hours).
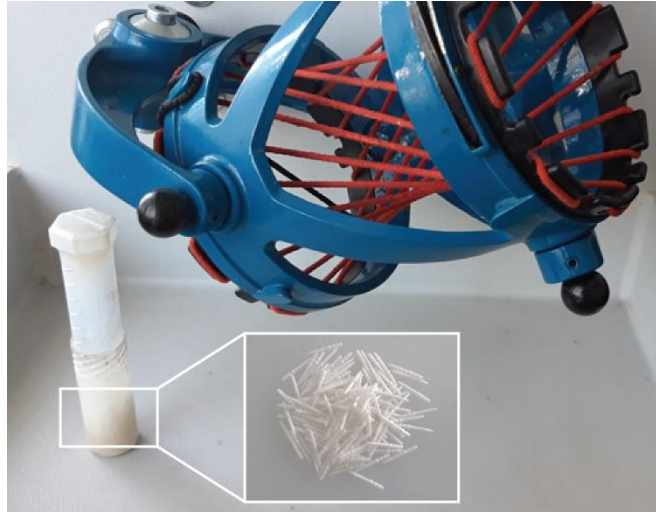
Figure 1. Photograph showing 3Y-TZP dental root posts (inset figure) and he plastic capsule containing 30 posts before mounting in Turbula mixer.

2.2. Characterisation

Morphological characterisation was performed on field-emission scanning electron microscopy (FEG-SEM; JSM 5310, JEOL, Tokyo, Japan) at accelerating voltage of 5 keV. The samples were carbon-coated before imaging.

The surface roughness has been characterised by Veeco Dimension 3000 atomic force microscope on three 10 x 10 µm areas per sample in tapping mode. Gwyddion software package [23] was used to evaluate surface parameters and produce surface plots after frequency split in order to separate waviness and roughness profile.

Randomly selected five fractured samples (lower straight part of the post; inset of Fig. 1) from each group were subjected to crystallographic phase analysis by X-ray diffraction (XRD) using Cu-Kα radiation over the range 27–37° 2θ (X'Pert PRO X-ray diffractometer, PANalytical, Almelo, TheNetherlands). Five samples were stacked together and fixated to an XRD holder using plasticine. The amount of XRD monoclinic zirconia fraction (X_m) was estimated using the Garvie and Nicholson method [24].

FIB-SEM sub-surface microstructural analyses were carried out on Helios NanoLab 650 (FEI, Hillsboro, OR, USA). A 0.5-mm-thick platinum coating was deposited onto the surface of interest using an ion beam assisted gas injection system at 30 kV and 0.43 nA to minimize the extensive curtaining effect. Across the selected interface regions, FIB milling was carried out using an ion beam at 30 kV and 65 nA, followed by ion polishing at 30 kV and 21 nA. Sub-surface areas were exposed and observed *in situ* under an angle of 52°, using an electron probe at 3 kV and 40-80 pA.

The forces at fracture of the posts were measured in a universal material-testing machine (Quasar 100, Galdabini, Cardano al Campo, Italy) using 3-point bending set-up. Weibull statistical analyses were conducted by using a ReliaSoft Weibull++ software package. After mechanical testing, the fracture surfaces of the broken 3Y-TZP posts were examined for fractographic details using FEG-SEM. The samples were carbon-coated before imaging.

3. Results

The microstructures of the lower, "pole" part of the 3Y-TZP post immediately after sintering (AS) and after 8 (8H), 50 (50H) and 200 (200H) hours of shaking in Turbula® mixer at 2 Hz rate are presented in Fig. 2. AS sample (Fig. 2a) exhibits typical 3Y-TZP microstructure composed of densely stacked polyhedral grains with monomondal grain size distribution. The average grain size was 0.65 µm. Low-magnification SEM (Supplementary data; Fig. S1) reveals that the surface is not flat but groovy as a consequence of the state of the surface of the steel mould for LPIM. 8 hours of shaking resulted in the distinct areas of sample 8H (Fig. 2b) that were flatten, where the grain boundaries were not clear anymore. One of the grains that was smashed by the impact was showing visible plastic deformation and cracking. Some tiny wear tracks were also observed, which were indicative of grinding effect from an obvious impact and slide scenario during shaking. The surface of 50H sample (Fig. 2c) exhibited large parts of a completely flattened surface, where grain boundaries of several neighbouring grains were obscured and with more extensive wear tracks as compared to the 50H sample (Fig. 2b). 200H sample (Fig. 2d) surface was similar to that of 50H but with the extended wear of the surface due to the impact and slide resulted in microchipping of the material from some of the grains.
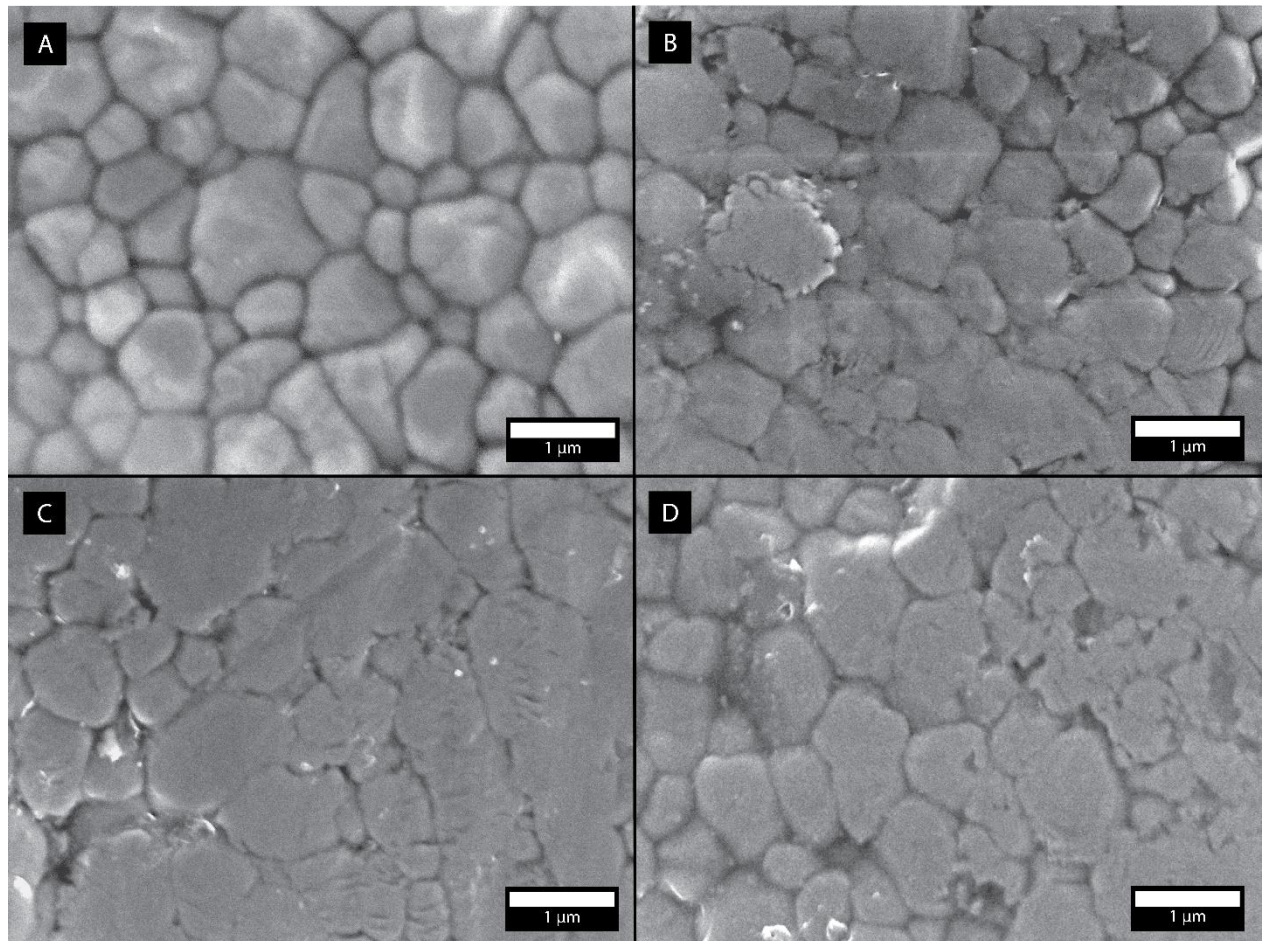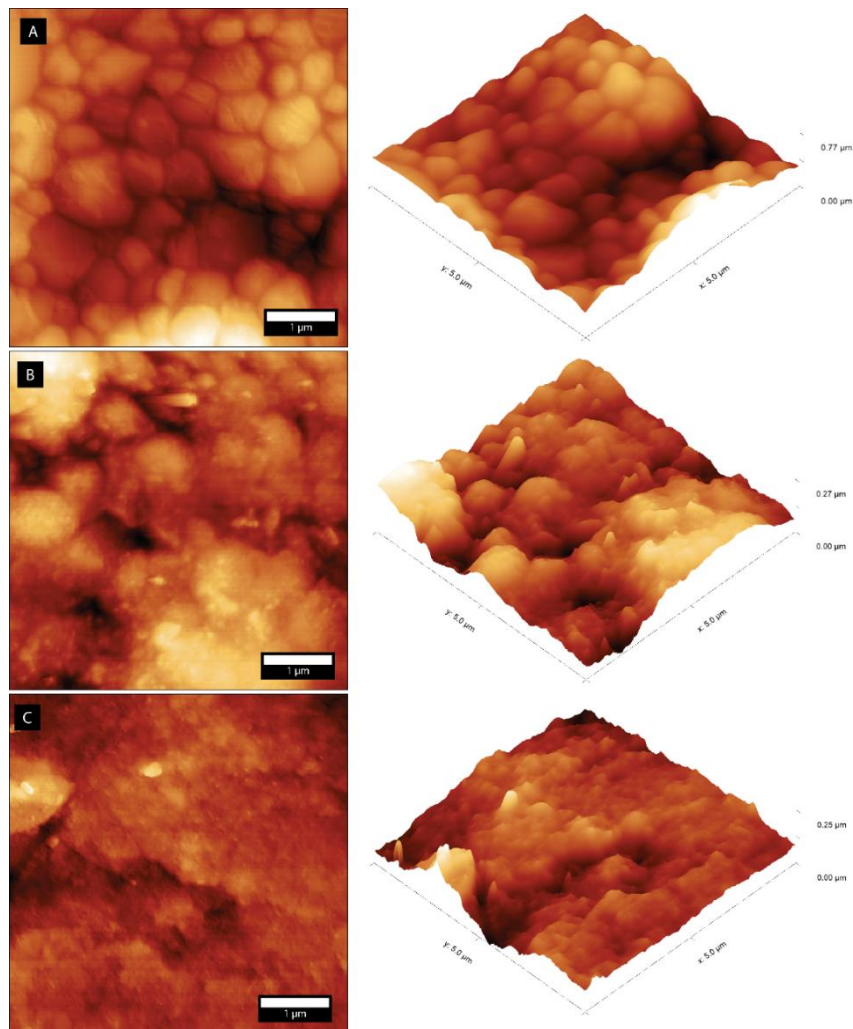

Figure 2. SEM micrographs showing representative surfaces of the (a) AS, (b) 8H, (c) 50H and (d) 200H samples.

It seemed that the higher amount of the surface of 200H sample was intact as compared to 50H, which could be the consequence of the surface irregularities, where different parts were locally subjected to a greater number of impacts depending on the surface roughness that was obviously inhomogeneous (inset of Fig. 2a).

AFM analysis was also performed to attain additional quantitative information from the effect of the impact and sliding during shaking of the 3Y-TZP posts. The results are presented in Figure 3 and Table 1. AS sample presented in Fig. 3a shows typical 3Y-TZP microstructure as seen in Fig. 2a, where some of the grains resembled hints of martensitic variants (monoclinic twinning). On the other hand, 3D image (right hand side of Fig. 3a) reveals the rough, groovy surface. 2D and 3D AFM micrographs of the 50H sample (Fig. 3b) show partly deformed surface where large parts of grains are flattened, and grain boundaries obscured. The surface of the 200H sample (Fig. 3c) is even more deformed and flattened as compared to the 50H sample (Fig. 3b).

Figure 3. AFM micrographs showing representative surfaces of the (a) AS, (b) 50H and (c) 200H samples.

In addition, surface roughness's were measured over single or over several grains to evaluate the effect of shaking time and/or the extent of impacting on the surface flattening. Both R_a's

were steadily decreasing with the time of shaking as a result of impact-induced surface flattening (Table 1). R_a over single grain decreased from about 18 to 4 nm, while R_a over several grains from 28 to 8 nm from AS to 500 H, respectively.

Table 1. AFM surface roughness measured over single or over several grains for the AS, 8H, 50H, 200H and 500H samples.

	R_a over single grain (nm)	R_a over grains (nm)
AS	18.6±5.8	28.1±5.5
8 h	7.3±1.6	13.8±2.1
50 h	7.2±2.9	18.9±3.8
200 h	5.7±1.5	10.4±3.3
500 h	4.2±1.3	8.4±1.1

XRD analysis showed that after sintering the posts consisted of tetragonal crystal structure typical for 3 mol.% yttria-doped zirconia (Fig. 4). With the increase in shaking time, several crystallographic features were observed in diffractograms. A slight emergence of the monoclinic zirconia phase was observed in all the samples (Fig 4a). The calculated XRD monoclinic fractions are listed in Table 2.

Table 2. XRD monoclinic fraction, X_m, and the intensity ratios of the tetragonal doublet peaks positioned around 35°

	X_m (%)	$I_{t(002)}/I_{t(110)}$
AS	3	0.62
8 h	9	0.98
50 h	7	1.03
200 h	6	1.10

As-sintered sample already contained 3 % of m-ZrO_2 that was also observed in Fig. 3a, as a result of the spontaneous *t-m* transformation of the partitioned yttria-lean *t*-ZrO_2 phase that had evolved during sintering at 1550 °C [11]. With shaking time, the content of *m*-ZrO_2 increased to 9 and 7 for 8H and 50H, respectively. It then decreased to 6 % for 200H sample. It is not clear whether the decrease can be assigned to the measurement scatter or to the fact that surface microchipping was observed for 200H samples (Fig. 2D). Besides, low-angle-2-theta-broadening accompanied with the decrease of intensity of the main tetragonal $(101)_t$ zirconia peak positioned at ~30° was observed (Fig 4a), that is also typical for ground or air-borne particle-abraded samples but to a lesser extent. Finally, the reversal of the intensities of the tetragonal doublet peaks positioned around 35° also evolved, as seen in Fig. 4b.
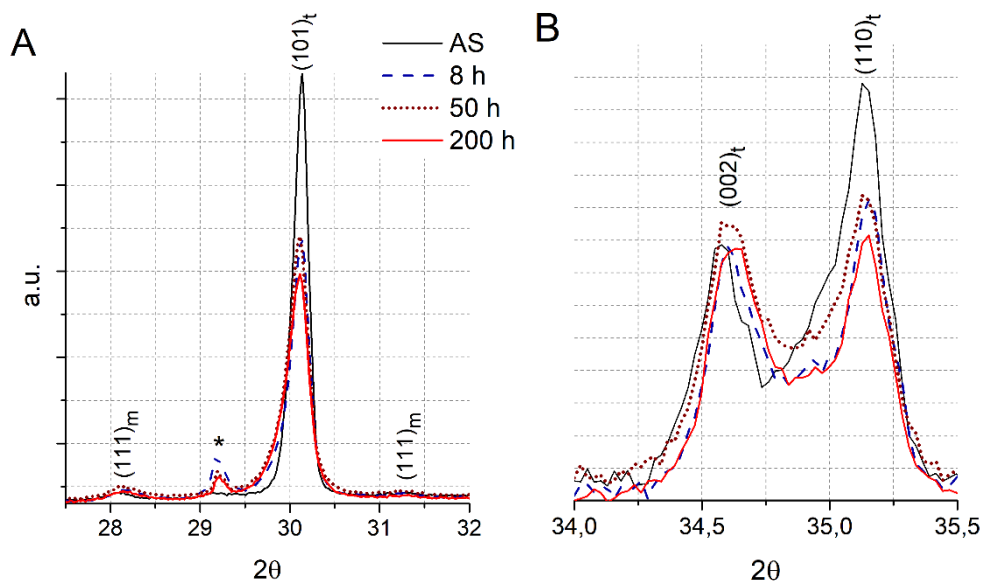
Figure 4. Representative XRD diffractograms of the 3Y-TZP dental root posts before and after shaking experiment presented at intersections of diffractograms at a) 27.5—32 2θ and b) 34—35.5 2θ. Asterisks indicates a reflection from the embedding material (plasticine).

Cross-sections prepared with SEM-FIB uncovered microstructural insight into the changes in the immediate sub-surface region upon shaking experiment, where extensive impact and sliding of the post surfaces occurred (Fig. 5). The as-sintered sub-surface was typical for 3Y-TZP material composed of equiaxed grains that differed in colour due to the orientation contrast (Fig. 5a). The top surface layer of grains indeed resembled hints of martensitic variants as indicated by red arrows that were also observed with AFM (Fig. 3a) and XRD (Fig 4a) analyses. After 8 h of shaking the surface on the right-hand side of the Fig. 5b was partly flattened with no discernible grain boundaries. Underneath this topmost 1 µm layer the grains were refined, again with no discernible grain boundaries and consisting of grey-featured dots scattered randomly across layer. In this layer a microcrak positioned parallel to the surface was observed as well (orange dotted circle). In other parts, going up to 6 µm in depth, individual grains are likewise deformed, but in a different way, i.e., featuring cleavage-like texturing (double black arrows) and newly-formed intragranular, sub-domains with boundaries of distinct contrast heterogeneities compared to its hosting grain (orange arrows). Distinct intra-granular contrast resembles multiple sub-domains. The cleavages in individual grains and the density of the shadows are less prominent as we traverse the cross-section from 6 µm downwards. Grains in this area also lack clear transition boundary. Similar altered subsurface microstructure was observed in samples shaked of longer times, however, in the presented case of 50H sample (Fig. 5c), the topmost 1 µm refined layer with no discernible grain boundaries was not detected. As already observed in different surface topographies (Fig 2), the initial surface irregularities in terms of roughness (Supplementary data; Fig. S1) may well lead to parts (as the bulgy one in Fig 5b) that were locally subjected to a greater number (and/or heavier) impacts leading to a more severe damage.
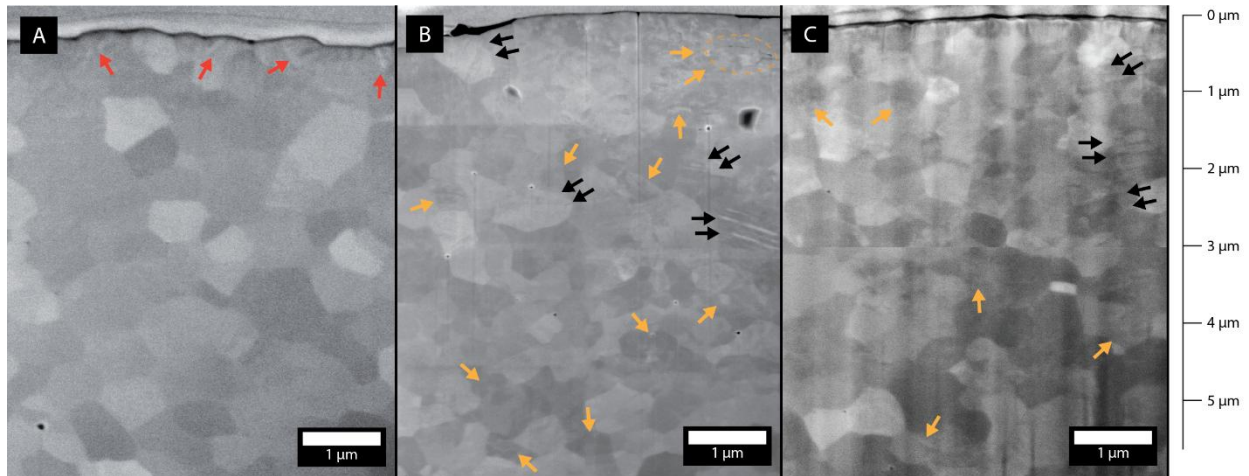
Figure 5. SEM-FIB cross-sectional micrographs of a) an as-sintered sample (AS) and a collage of micrographs (for attaining better resolution) depicting the topmost ~6 μm of samples after b) 8 (8H) and c) 50 hours (50H) of shaking, respectively. Red arrows are indicating the formation of martensitic variants. Orange dotted circle and arrows are indicating on a microcrak and intragranular, sub-domains, respectively. Black double arrows are indicating on cleavage-like texturing of the grains.

The results of the bending strengths of all the posts before and after shaking experiment are presented in Figure 6. The bending strengths of as-sintered samples had a mean force at fracture of 71 N. With shaking time, the mean value of force at fracture steadily increased, i.e., from 80 to 101 N for 2 to 100 hours of shaking, respectively, indicating on the effect of an apparent impact strengthening of 3Y-TZP. Substantially longer periods of shaking time (number of impacts) did not, however, resulted in further increase nor decrease in the mean force at fracture that was around 106 N for 200 and 500 hours.
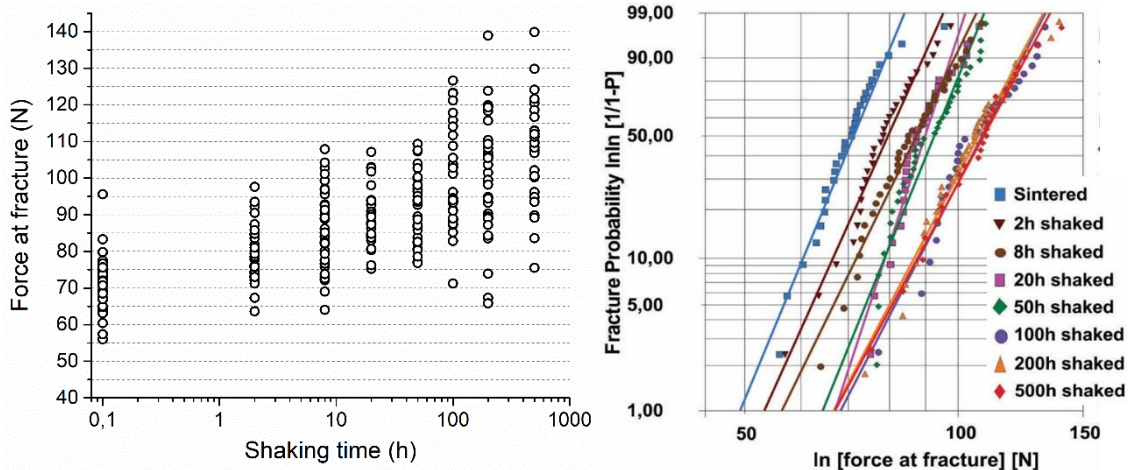

Figure 6. a) 3-point flexural strength data (force at fracture in Newtons) and b) corresponding Weibull plot for fractured samples before and after shaking experiment with the various time of shaking.

Those mean values represent a ~51 % increase in fracture strength. The results of the Weibull statistical analysis of the fracture load data are presented in Fig. 6b and Table 3, wherein the latter two characteristic parameters for each test group, the characteristic fracture load, S_q, and the Weibull modulus, m, are given. Results clearly indicate that with the increase in the shaking time the characteristic fracture load steadily increases with an initial value of 74 N and reaches a

plateau at 112 N as also observed in Fig. 6a. However, the Weibull modulus slightly decreases from an initial value of 11.5 to 8.8 for AS and 500H groups, respectively. The exceptions from this trend were 20H and 50H groups.

Table 3. Calculated statistical parameters for the Weibull distributions of fractured samples before and after several hours of shaking.

	m	s_q (MPa)
AS	11.5	74
2 h	10.5	83
8 h	9.7	91
20 h	14.5	92
50 h	11.7	96
100 h	9.2	112
200 h	9.0	111
500 h	8.8	113

SEM examination of fractured surfaces of the representative specimens in Figs. 7–8 revealed several fractographic features that are typically encountered on fractured surfaces of polycrystalline ceramics. Within the majority of the specimens, a surface-type of fracture origin was observed irrespective of the additional shaking protocol used (Fig. 7). On the specimens with the lowest force at fracture, a volume-type of fracture origin was observed to govern the strength (Fig. 8). In all the fractures, as seen in Fig. 7, the mist was not recognisable, but the early coarse microstructural hackle lines running away from the fracture origin were identified in all the cases.
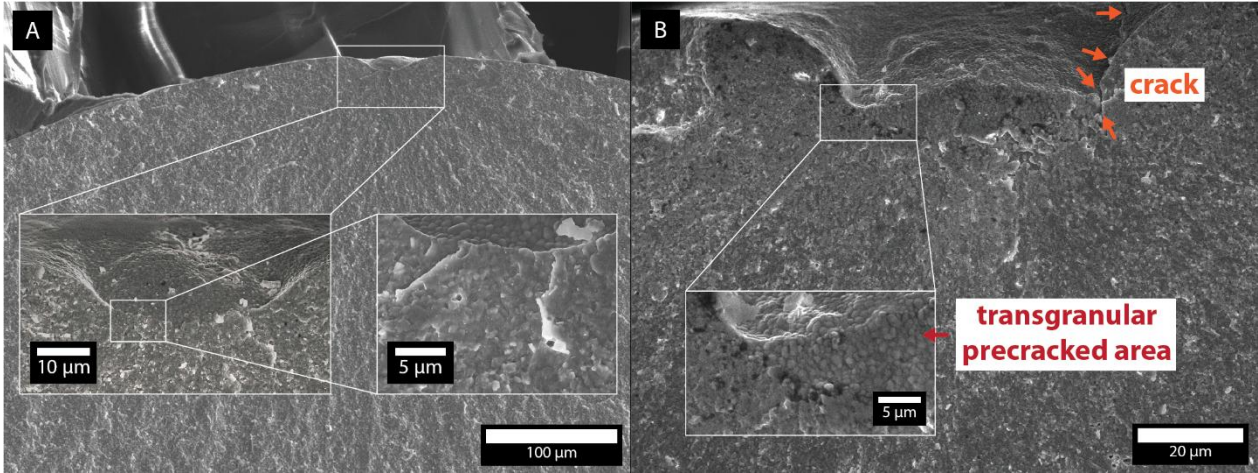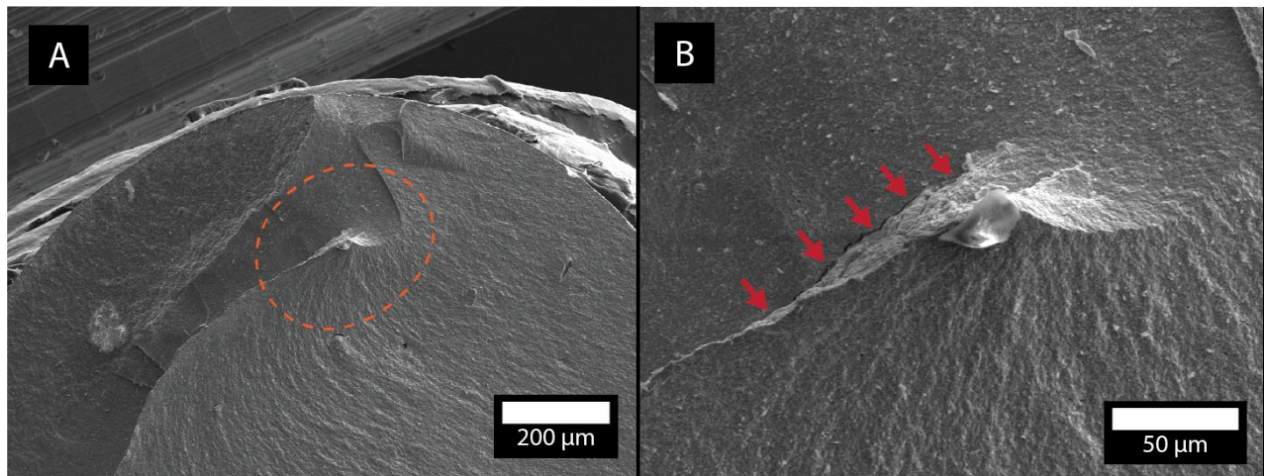

Figure 7. SEM fractographic analyses of the samples from AS group with surface-type of fracture origin fracturing at a) 110 N of bending stress or b) lower.

The surface fracture origin was identical for all the inspected samples. It was in the form of spherical/globular imprint (left-hand side inset of Fig. 7a) originating from the surface irregularity of the steel mould after the green body was extracted during the LPIM process. The AS samples with the highest force at fracture exhibited a sharp edge running down from the imprint, where the crack was initiated, into the bulk, with a predominant transgranular fracture surface typical for 3Y-TZP (right-hand side inset of Fig. 7a). AS samples with lower force at fracture possessed the same surface imprint, however, it contained a pre-crack, i.e., an precrack running around the spherical part into the bulk (light red arrows in Fig. 7b) obviously present already prior to the sintering process due to the clear observation of edge cracking and region of intergranular fracture with a half-penny type of geometry (inset of Fig. 7b). These type of surface fracture origins were also observed in other samples that underwent an extended time of shaking, where the effect of impact and sliding of the 3Y-TZP posts provided an extensive strengthening of the post. For the lowest forces at fracture, a volume-type of defects, as presented in Fig. 8 (dotted red circle in Fig. 8a). It was in the form of a ~100 μm long crack (red arrows in Fig.8b). This kind of fracture origin did prevailed over the effect of strengthening since specimens containing it where stranded off from the population remaining at the lower bottom of measured forces at fracture (Fig. 6a). This explains the reason for exceptionally high Weibull moduli for the 20H and 50H, since these populations samples did not contain ones with the volume-type of the flaw as observed in Fig. 8.

Figure 8. a) Lower and b) higher magnification SEM microgprahs showing fractographic analysis of the sample from AS group with volume-type of fracture origin. (fracturing at 57 N of bending stress).

4. Discussion

The prolong shaking of the 3Y-TZP dental root posts performed in a Turbula mixer up to 500 hours with a 2 Hz rate, where a continuous and pronounced impact and wear sliding between the posts resulted in the gradual flattening of the 3Y-TZP surface (Fig. 2). For a relatively short shaking time, such as in the sample 50H, the 3Y-TZP surface alteration was to an extent similar to polishing induced surface smear layer, however, on a micron-sized scale (Fig. 2c). Likewise, the grains were flattened out and the grain boundaries diminished in the process of plastic deformation as a result of the impact between posts. The decrease in surface roughness to

several nanometers (Table 1) was indeed similar to the one measured for a polished 3Y-TZP surface [25]. With the prolonged shaking times, the intensification of the impact sliding process lead to the surface alteration switching from plastic to plastic/brittle deformation, where parts from the grains were chipped out or delaminated (Fig. 2d). This was indicative on pronounced local contact stress between two impacting posts, where the stresses were magnified upon contact through a relatively small area of contact as a result of an uneven, rough surface with only several grains exposed. Before microchipping and spallation of the surface, there were features observed (Fig. 2c) that could be a sign of a partial Hertzian cone cracking [26], but beside microchipping no subsurface (micro)cracks were observed with FIB (Fig. 5) or after fracture (Fig. 8). Quasi-plastic deformation in zirconia-based ceramics does occur as a result of subsurface shear stresses and/or tetragonal-to-monoclinic phase transformation. Thus, the surface alteration on a micro-scale during the shaking experiment was to a limited extent similar to microstructural changes encountered during grinding/polishing of densely sintered Y-TZP ceramics that causes plastic-to-brittle damage to the surface depending on the variation of the grinding/polishing parameters [27].

The resultant surface damage affected the microstructural phase composition as measured with the XRD (Figure 4). Interestingly, only a small proportion of the monoclinic phase was detected not exceeding 10 % of the calculated XRD monoclinic fraction. Such low value yields a transformation depth of less than 300 nm [28]. The rather low amount of the transformed monoclinic fraction evolved after impacting during shaking experiment is well in agreement with studies on the ground [29][30] and sandblasted [7][31][21][32] zirconia. The observed asymmetric low-2-theta broadening of (111)c\(101)t peak is characteristic of mechanical treatment, characteristic for airborne-particle abrasion [7] or grinding. Hasegawa [33] and Kitano et al. [34] postulated that such distortion of the peaks is associated with the stress-induced phase transformation of tetragonal (t-r) or cubic (c-r) to rhombohedral zirconia that can occur during surface abrasion in the partially stabilised as well as in fully stabilised zirconia with 2—5 mol.% and 5—10 mol.% of yttria, respectively. c-r phase transformation was also observed in the fully stabilised samples (10 mol.% of yttria) that underwent ion implantation of [15]N.[35] The r-ZrO_2 phase is thought to exist only in the surface layer under some stress, since it can be removed by polishing. In addition, the stress subsurface layer was successfully removed by annealing between 800—1000 °C.[26] On the other hand, Kondoh [37] contradicted the rhobohedral phase existence and assigned the so-called hump, i.e., the low-2-theta asymmetric broadening of the $(111)_c$\$(101)_t$ peaks, in 2-15YSZ materials to lattice distortion. However, it was not clear how the samples were sintered nor why the asymmetry was observed already after sintering. Thermal ageing for 1000 hours at 1073 to 1273 K could annihilate the observed distortion, which reappeared after thermal ageing at higher temperatures up to 1573 K. In the present case, additional feature observed in diffractogram for the shaked samples was in the reversed intensities of the tetragonal doublet peaks, positioned around 35° 2-theta (Fig. 4b), i.e., $I_t(002)/I_t(110)$, which had increased from 0.6 for AS sample to more than 1 for samples shaked for 50 h or longer shaking times (Table 2). The observed increase in the $I_t(002)/I_t(110)$ ratio might be associated with the ferroelastic domain (FE) switching, which is known to occur as a result of an externally applied stress [38].

The subsurface microstructure observed with the SEM-FIB (Figure 5) of the sample that underwent shaking resembled a deformed subsurface region consisting of the complex gradient with features that are to an extent similar to the ones observed after sandblasting of 3Y-TZP [7][31][21] or grinding [29]. One part that was heavily deformed consisted of the refined grains

with no discernible grain boundaries and a lateral microcrack (Fig.5b). In general, however, irrespective of the time of the shaking the altered subsurface 6 µm thick layer was composed from individually deformed grains that either featured a cleavage-like texturing or newly-formed intragranular, sub-domains with boundaries of distinct contrast heterogeneities compared to its hosting grain (Fig 5b-c). It was impossible to discern from the observed features between the monoclinic phase and the possible rhombohedral phase formation or even FE domain switching. It was shown by Munõz-Tabares et al. [29] when performing grazing incidence XRD of ground 3Y-TZP that the asymmetry of the main peak at 30° had increased, apparently consisted of two convoluted peaks, whereas the tetragonal doublet at 35° disappeared forming a single peak at lowered angles, all being assigned to the rhombohedral phase. In the case of ground [29] or scratched and indented [39] 3Y-TZP surfaces, deeper from the nanograin layer, highly distorted microstructures were observed with TEM, i.e., high density of dislocations and Moiré patterns that had accumulated at the boundary between martensite plates. Only a limited amount of the monoclinic phase was detected in the present study (Fig. 4, Table 2).

Cleavage-like texturing and newly-formed intragranular sub-domains expending up to 6 µm in depth observed in Fig. 5b-c could be tentatively assigned to the presence of FE domains. For instance, Mercer et al. [40] showed a presence of several fine FE twin domains of two orthogonal orientations within a plastic zone of indented (with Vickers prism) 4 mol.% yttria-stabilised (t˙) zirconia. Baither et al. [41] showed dislocation structure consisted of intersecting dislocations on different slip systems with strongly bowed-out segments in the tetragonal (t˙) zirconia when deformed in compression along an orientation at various temperatures between 500 and 1400 °C. The observed microstructure prevented recovery with the high measured temperature invariant coercive stress of up to 700 MPa. The rearrangement of the FE domains to orthogonal two directions was shown with XRD also in the 3Y-TZP system, where the amount of switching increased with increasing the applied stress and remained with loading time [42]. The critical stress required for FE to operate decreased with increasing temperature with the activation energy to be 16 kJ/mol.

Additional microanalyses studies will, however, be necessary in order to fully understand the microstructural features observed in Fig 5 for their relation to the possible FE switching. Nevertheless, the observed reversal of the intensities of the two tetragonal doublet peaks (Fig. 4b) is indeed characteristic for FE domain switching. On the other hand, the ~51 % increase in the fracture strength (Figure 6, Table 3) of 3Y-TZP posts as a result of the shaking time is indicative of substantial evolution of compressive residual stresses. According to the above literature discussed, substantial coercive stresses acting in a compressive manner can be activated on the account of FE domain switching especially in the events of extensive impact and sliding scenarios, where shear and compression forces take place. The impacting of the posts during shaking also triggered the t-m transformation, which could well add up to the magnitude of the evolved compressive microresidual stresses; however, only limited amount of the monoclinic phase was recorded (Table 2). Moreover, no distinct monoclinic twin variants nor microcracks were observed (Fig. 5b). Interestingly, Chintapalli et al. [32] correlated the limited amount of t-m transformation in the sandblasted 3Y-TZP to the contribution of compressive residual stresses in the 450—800 MPa range based on XRD and Raman data. It was later shown by Cotič et al. [7], however, comparing the effect of sandblasting and hydrothermal ageing on the biaxial flexural strength that sandblasting yielded a 43.6 % increase in strength, while hydrothermal ageing alone could contribute to a maximum increase in average strength of 20.8 %. In the latter case, the amount of the monoclinic phase was >50 % (in comparison to >5

% for the sandblasted specimen) with the coherent *t-m* transformed 10-micrometre-thick layer evolved.

The evolved compressive residual stress zone after shaking experiment contributed to a systematic increase in the bending strength of the posts (Figure 6a). The characteristic fracture loads needed for the posts to fracture obtained from the Weibull analysis were indeed gradually increased from 74 N, reaching a saturation point after 100 h of shaking at 111 N (Table 3). The Weibull modulus slightly decreased as a result of the wider range of forces at fracture per population indicating on the different type of the characteristic surface flaws responsible for fracture. Even though all the surface critical extrinsic flaws originated from the identical irregularity of the mould for LPIM (Fig 7a), the fact how deleterious they were depended on the demoulding. It followed that some of the imprints were completely restricted to the surface. Some of these spherical imprints were rounded and prenotched with Hertzian cone types of cracks (Fig. 7b). The most critical volume type of flaws in the form of 100-micron-sized long cracks in the centre of the post contributed to the lowest fracture strength values. These were only recognised in those samples protruding out on the lower side of the population (Fig. 6a). Samples containing such flaws received limited strength increase and as such were insensitive to the beneficial evolution of compressive residual stresses after shaking. Sample population not having such type of flaws had atypical high Weibull moduli (Table 3).

5. Conclusions

The present work evaluated the effects of continuous impacting between 3Y-TZP root posts during up to 500-hour-long shaking performed in a Turbula mixer, where a continuous and pronounced impact and wear sliding between the posts occurred. The following conclusions are made:

(1) The prolong shaking resulted in the gradual flattening of the 3Y-TZP surfaces and a decrease in surface roughness to several nanometers. The surface variation was similar to polishing inducing a surface smear layer. The longest shaking times induced partial microchipping and spallation of the surface grains.

(2) Shaking resulted in the alteration of the XRD diffractograms, where low-angle-2-theta-broadening of the main tetragonal $(101)_t$ zirconia peak positioned at ~30° and pronounced reversal of intensities of the tetragonal doublet peaks positioned around 35° were observed. The latter was indicative of the ferroelastic domain switching. Only limited amounts, X_m (6-9 wt.%), of the monoclinic phase were detected.

(3) The subsurface microstructure observed after shaking showed a deformed, altered 6-micrometre-thick subsurface region consisting of the complex microstructure with various features. It consisted of individual grains with cleavage-like texturing and/or newly-formed intragranular, sub-domains with boundaries of distinct contrast heterogeneities, as compared to the hosting grain.

(4) The evolution of compressive residual stress in the subsurface region after shaking experiment contributed to a substantial, systematic increase (~51 %) in the bending strengths of the posts. According to Weibull analysis, the characteristic fracture load steadily increased with an initial value of 74 N reaching a saturation/plateau at 112 N after 100 h shaking. However, the Weibull modulus slightly decreased from an initial value of 11.5 to 8.8 for AS and 500H groups, respectively.

(5) Fractographic analysis showed the majority of the critical flaws were of extrinsic surface type of flaws originating from the irregularity of the mould for LPIM imprinted during the demoulding process. Some of the imprints were completely restricted to the surface, while other spherical imprints were rounded with Hertzian cone types of cracks. Several volume types of flaws in the form of long cracks in the centre of the post were also observed. These had contributed to the lowest forces of fracture values that were insensitive to the substantial strength increase after shaking.

Acknowledgements

References

[1]   I. Denry, J.R. Kelly, State of the art of zirconia for dental applications., Dent. Mater. 24 (2008) 299–307. doi:10.1016/j.dental.2007.05.007.

[2]   R. Garvie, R. Hannink, R. Pascoe, Ceramic steel?, Nature. 258 (1975) 703–704. http://www.nature.com/nature/journal/v258/n5537/abs/258703a0.html (accessed November 12, 2013).

[3]   K. Kobayashi, H. Kuwajima, T. Masaki, Phase change and mechanical properties of ZrO2-Y2O3 solid electrolyte after ageing, Solid State Ionics. 3–4 (1981) 489–493. doi:10.1016/0167-2738(81)90138-7.

[4]   S. Lawson, Environmental degradation of zirconia ceramics, J. Eur. Ceram. Soc. 15 (1995) 485–502. doi:10.1016/0955-2219(95)00035-S.

[5]   J. Chevalier, L. Gremillard, A. V. Virkar, D.R. Clarke, The Tetragonal-Monoclinic Transformation in Zirconia: Lessons Learned and Future Trends, J. Am. Ceram. Soc. 92 (2009) 1901–1920. doi:10.1111/j.1551-2916.2009.03278.x.

[6]   M. Keuper, K. Eder, C. Berthold, K.G. Nickel, Direct evidence for continuous linear kinetics in the low-temperature degradation of Y-TZP, Acta Biomater. 9 (2013) 4826–4835. doi:10.1016/j.actbio.2012.08.032.

[7]   J. Cotič, P. Jevnikar, A. Kocjan, Ageing kinetics and strength of airborne-particle abraded 3Y-TZP ceramics, Dent. Mater. 33 (2017) 847–856. doi:10.1016/j.dental.2017.04.014.

[8]   M. Keuper, C. Berthold, K.G. Nickel, Long-time aging in 3 mol.% yttria-stabilized tetragonal zirconia polycrystals at human body temperature, Acta Biomater. 10 (2014) 951–959. doi:10.1016/j.actbio.2013.09.033.

[9]   L. Ruiz, M.J. Readey, Effect of heat-treatment on grain size, phase assemblage, and mechanical properties of 3 mol% Y-TZP, J. Am. Ceram. Soc. 79 (1996) 2331–2340. doi:10.1111/j.1151-2916.1996.tb08980.x.

[10]   T. Kosmač, A. Kocjan, Ageing of dental zirconia ceramics, J. Eur. Ceram. Soc. 32 (2012) 2613–2622. doi:10.1016/j.jeurceramsoc.2012.02.024.

[11]   D. Bučevac, T. Kosmač, A. Kocjan, The influence of yttrium-segregation-dependent phase partitioning and residual stresses on the aging and fracture behaviour of 3Y-TZP ceramics, Acta Biomater. 62 (2017) 306–316. doi:10.1016/j.actbio.2017.08.014.

[12]   F. Zhang, M. Batuk, J. Hadermann, G. Manfredi, A. Mari??n, K. Vanmeensel, M. Inokoshi, B. Van Meerbeek, I. Naert, J. Vleugels, Effect of cation dopant radius on the hydrothermal stability of tetragonal zirconia: Grain boundary segregation and oxygen vacancy annihilation, Acta Mater. 106 (2016) 48–58. doi:10.1016/j.actamat.2015.12.051.

[13]   A. Samodurova, A. Kocjan, M. V Swain, T. Kosmač, The combined effect of alumina and silica co-doping on the ageing resistance of 3Y-TZP bioceramics., Acta Biomater. 11 (2015) 477–87. doi:10.1016/j.actbio.2014.09.009.

[14]   P. Jevnikar, M. Golobič, A. Kocjan, T. Kosmač, The effect of nano-structured alumina coating on the bond strength of resin-modified glass ionomer cements to zirconia ceramics, J. Eur. Ceram. Soc. 32 (2012) 2641–2645. doi:10.1016/j.jeurceramsoc.2012.03.037.

[15]   M. Kern, Bonding to oxide ceramics - Laboratory testing versus clinical outcome, Dent. Mater. 31 (2015) 8–14. doi:10.1016/j.dental.2014.06.007.

[16]   J. Cotič, P. Jevnikar, A. Kocjan, T. Kosmač, Complexity of the relationships between the sintering-temperature-dependent grain size, airborne-particle abrasion, ageing and strength of 3Y-TZP ceramics, Dent. Mater. 32 (2016) 510–518. doi:10.1016/j.dental.2015.12.004.

[17]   T. Kosmac, C. Oblak, P. Jevnikar, N. Funduk, L. Marion, The effect of surface grinding and sandblasting on flexural strength and reliability of Y-TZP zirconia ceramic., Dent. Mater. 15 (1999) 426–33. http://www.ncbi.nlm.nih.gov/pubmed/10863444.

[18]   F.F. Lange, A.G. Evans, Erosive Damage Depth in Ceramics: A Study on Metastable, Tetragonal Zirconia, J. Am. Ceram. Soc. 62 (1979) 62–65. doi:10.1111/j.1151-2916.1979.tb18807.x.

[19]   T. Kosmač, Č. Oblak, L. Marion, The effects of dental grinding and sandblasting on ageing and fatigue behavior of dental zirconia (Y-TZP) ceramics, J. Eur. Ceram. Soc. 28 (2008) 1085–1090. doi:10.1016/j.jeurceramsoc.2007.09.013.

[20]   J. a. Muñoz-Tabares, E. Jiménez-Piqué, M. Anglada, Subsurface evaluation of hydrothermal degradation of zirconia, Acta Mater. 59 (2011) 473–484. doi:10.1016/j.actamat.2010.09.047.

[21]   C.F. Caravaca, Q. Flamant, M. Anglada, L. Gremillard, J. Chevalier, Impact of sandblasting on the mechanical properties and aging resistance of alumina and zirconia based ceramics, J. Eur. Ceram. Soc. 38 (2018) 915–925.

doi:10.1016/j.jeurceramsoc.2017.10.050.

[22] S. Jovanovski, J. Cotič, A. Kocjan, Č. Oblak, P. Jevnikar, Fracture resistance of endodontically treated maxillary incisors restored with zirconia posts: effect of the internal plateau preparation, Adv. Appl. Ceram. 118 (2019). doi:10.1080/17436753.2018.1508625.

[23] D. Nečas, P. Klapetek, Gwyddion: An open-source software for SPM data analysis, Cent. Eur. J. Phys. 10 (2012) 181–188. doi:10.2478/s11534-011-0096-2.

[24] R. Garvie, P. Nicholson, Structure and Thermomechanical Properties of Partially Stabilized Zirconia in the CaO-ZrO2 System, J. Am. Ceram. S. 55 (1972) 152–157. http://onlinelibrary.wiley.com/doi/10.1111/j.1151-2916.1972.tb11241.x/abstract (accessed April 19, 2013).

[25] P. Jevnikar, K. Krnel, A. Kocjan, N. Funduk, T. Kosmac, The effect of nano-structured alumina coating on resin-bond strength to zirconia ceramics., Dent. Mater. 26 (2010) 688–96. doi:10.1016/j.dental.2010.03.013.

[26] M. Swain, Unstable cracking (chipping) of veneering porcelain on all-ceramic dental crowns and fixed partial dentures., Acta Biomater. 5 (2009) 1668–77. doi:10.1016/j.actbio.2008.12.016.

[27] R.G. Luthardt, M.S. Holzhüter, H. Rudolph, V. Herold, M.H. Walter, CAD/CAM-machining effects on Y-TZP zirconia, Dent. Mater. 20 (2004) 655–662. doi:10.1016/j.dental.2003.08.007.

[28] T. Kosmać, R. Wagner, N. Claussen, X-Ray Determination of Transformation Depths in Ceramics Containing Tetragonal ZrO2, J. Am. Ceram. Soc. 64 (1981) c-72-c-73. doi:10.1111/j.1151-2916.1981.tb10285.x.

[29] J. a. Muñoz-Tabares, E. Jiménez-Piqué, J. Reyes-Gasga, M. Anglada, Microstructural changes in ground 3Y-TZP and their effect on mechanical properties, Acta Mater. 59 (2011) 6670–6683. doi:10.1016/j.actamat.2011.07.024.

[30] J.J. Roa, M. Turon-vinas, M. Anglada, Surface grain size and texture after annealing ground zirconia, J. Eur. Ceram. Soc. 36 (2016) 1519–1525. doi:10.1016/j.jeurceramsoc.2015.12.022.

[31] R.K. Chintapalli, F.G. Marro, E. Jimenez-Pique, M. Anglada, Phase transformation and subsurface damage in 3Y-TZP after sandblasting., Dent. Mater. 29 (2013) 566–72. doi:10.1016/j.dental.2013.03.005.

[32] R.K. Chintapalli, A. Mestra Rodriguez, F. Garcia Marro, M. Anglada, Effect of sandblasting and residual stress on strength of zirconia for restorative dentistry applications., J. Mech. Behav. Biomed. Mater. 29 (2014) 126–37. doi:10.1016/j.jmbbm.2013.09.004.

[33] H. Hasegawa, Rhombohedral phase produced in abraded surfaces of partially stabilized zirconia (PSZ), J. Mater. Sci. Lett. 2 (1983) 91–93. http://www.springerlink.com/index/m244uqq288381217.pdf (accessed April 19, 2013).

[34] Y. Kitano, Y. Mori, Rhombohedral Phase in Y2O3-Partially-Stabilized ZrO2, J. Am. Ceram. Soc. 71 (1988) C-34-C–36. http://onlinelibrary.wiley.com/doi/10.1111/j.1151-2916.1988.tb05776.x/abstract (accessed April 19, 2013).

[35] H. Hasegawa, T. Hioki, O. Kamigaito, Cubic-to-rhombohedral phase transformation in zirconia by ion implantation, J. Mater. Sci. Lett. 4 (1985) 1092–1094. http://www.springerlink.com/index/u82h270514772thp.pdf (accessed April 19, 2013).

[36] Y. Kitano, Y. Mori, A. Ishitani, T. Masaki, Structural Changes by Mechanical and Thermal Stresses of 2.5-mol%-Y2O3-Stabilized 2.5-mol%-Y2O3-Stabilized Tetragonal Zr02 Polycrystals, J. Am. Ceram. Soc. 71 (1988) C-382-C383.

[37] J. Kondoh, Origin of the hump on the left shoulder of the X-ray diffraction peaks observed in Y2O3-fully and partially stabilized ZrO2, J. Alloys Compd. 375 (2004) 270–282. doi:10.1016/j.jallcom.2003.11.129.

[38] A. Virkar, R. Matsumoto, Ferroelastic domain switching as a toughening mechanism in tetragonal zirconia, J. Am. Ceram. Soc. 69 (1986) C-224-C–226. http://onlinelibrary.wiley.com/doi/10.1111/j.1151-2916.1986.tb07341.x/abstract (accessed January 6, 2014).

[39] J. a. Muñoz-Tabares, E. Jiménez-Piqué, J. Reyes-Gasga, M. Anglada, Microstructural changes in 3Y-TZP induced by scratching and indentation, J. Eur. Ceram. Soc. 32 (2012) 3919–3927. doi:10.1016/j.jeurceramsoc.2012.02.026.

[40] C. Mercer, J.R. Williams, D.R. Clarke, A.G. Evans, On a ferroelastic mechanism governing the toughness of metastable tetragonal-prime (t′) yttria-stabilized zirconia, Proc. R. Soc. A Math. Phys. Eng. Sci. 463 (2007) 1393–1408. doi:10.1098/rspa.2007.1829.

[41] D. Baither, M. Bartsch, B. Baufeld, A. Tikhonovsky, A. Foitzik, M. Rühle, U. Messerschmidt, Ferroelastic and Plastic Deformation of t′-Zirconia Single Crystals, J. Am. Ceram. Soc. 84 (2004) 1755–1762. doi:10.1111/j.1151-2916.2001.tb00911.x.

[42] T. Kiguchi, W. Urushihara, A. Saiki, K. Shinozaki, N. Mizutani, Effect of stress and temperature on ferroelastic domain switching of partially stabilized zirconia pseudo-single crystals, Nippon Seramikkusu Kyokai Gakujutsu Ronbunshi/Journal Ceram. Soc. Japan. 104 (1996) 529–534. doi:10.2109/jcersj.104.529.

Electronic Annex

*Declaration of Interest Statement

Declaration of interests

☒ The authors declare that they have no known competing financial interests or personal relationships that could have appeared to influence the work reported in this paper.

☐The authors declare the following financial interests/personal relationships which may be considered as potential competing interests: